

RSC Advances



This is an *Accepted Manuscript*, which has been through the Royal Society of Chemistry peer review process and has been accepted for publication.

Accepted Manuscripts are published online shortly after acceptance, before technical editing, formatting and proof reading. Using this free service, authors can make their results available to the community, in citable form, before we publish the edited article. This *Accepted Manuscript* will be replaced by the edited, formatted and paginated article as soon as this is available.

You can find more information about *Accepted Manuscripts* in the [Information for Authors](#).

Please note that technical editing may introduce minor changes to the text and/or graphics, which may alter content. The journal's standard [Terms & Conditions](#) and the [Ethical guidelines](#) still apply. In no event shall the Royal Society of Chemistry be held responsible for any errors or omissions in this *Accepted Manuscript* or any consequences arising from the use of any information it contains.

Graphene-analogue Boron Nitride/Ag₃PO₄ composite for efficient visible-light-driven photocatalysis

Yanhua Song^{a,b}, Hui Xu^{a*}, Cheng Wang^a, Jijia Chen^a, Jia Yan^a, Yuanguo Xu^a, Yeping Li^a, Chengbao Liu^c, Huaming Li^a, Yucheng Lei^{a,*}

^a School of Materials Science & Engineering, Institute for Energy Research, Jiangsu University, Zhenjiang 212013, P. R. China

^b Jiangsu University of Science and Technology, Zhenjiang 212003, P. R. China

^c Jiangsu Key Laboratory for Environment Functional Materials, Suzhou University of Science and Technology, Suzhou 215009, P. R. China

**Corresponding author: Tel.:+86-0511- 88791800; Fax: +86-0511- 88791800*

E-mail address: xh@ujs.edu.cn; yplei@ujs.edu.cn

Abstract: Graphene-analogues BN modified Ag₃PO₄ photocatalysts were successfully prepared. The composites were characterized by X-ray diffraction (XRD), X-ray photoelectron spectroscopy (XPS), transmission electron microscopy (TEM), scanning electron microscopy (SEM), UV-visible diffuse reflectance spectroscopy (DRS), fourier transformed infrared (FT-IR) spectroscopy and photoelectrochemical experiment. The results showed that after adding a small amount of graphene-analogue BN, the composite photocatalysts exhibited significantly enhancing photocatalytic activity and good stability for the photocatalytic degradation of RhB. The 0.5 wt.% BN content sample showed the best photocatalytic activity. The photocatalytic efficiency enhancement of the graphene-analogue BN/Ag₃PO₄ photocatalyst could be attributed to the synergetic role between graphene-analogue BN and Ag₃PO₄, which suppressed the recombination of photogenerated electron-hole pairs. It was found that the photocatalytic degradation of RhB by the photocatalyst

followed pseudo-first-order kinetics. The photocatalytic mechanism of the graphene-analogue BN/Ag₃PO₄ composite was also investigated.

Keywords: Graphene-analogues BN; Ag₃PO₄; Photocatalytic; Composite

1. Introduction

Photocatalytic technology has been used widely in solar energy conversion and environmental protection because it represents an easy way to utilize the energy of solar light and is a promising, environmental, cost-effective method.¹⁻³ Design and development of photocatalysts is the core issue in the photocatalytic technology.⁴ Recently, new photocatalysts, such as Ag-based,⁵ Tantalum-based,⁶ W-based semiconductors⁷ have been fabricated in order to overcome the drawbacks of the traditional TiO₂ materials. Despite many of these semiconductor photocatalysts being effective for the photocatalytic degradation of environment organic pollutants and water splitting, the present investigation are still far from the ideal goal. Therefore, the present situation in the photocatalysis study needs the researchers to continue develop semiconductor materials with the innovative, efficient and high stability.

Ag₃PO₄ used as an Ag-based semiconductor exhibits extremely high photooxidative capabilities for O₂ evolution from water and organic contaminant degradation under visible light irradiation.⁸⁻¹⁰ However, the further application of Ag₃PO₄ is limited due to its own defects, including the poor stability in photocatalysis process and low specific surface area. In order to solve its self issue, many efforts have been proposed. For one thing, the researchers improved the photocatalytic

activity through the modification on the shape, morphology, and crystal face of Ag_3PO_4 crystals.¹¹⁻¹³ For the other thing, coupling Ag_3PO_4 with other semiconductor photocatalysts could be regarded as a good strategy to obtain efficient and stable photocatalysts.¹⁴ There are many Ag_3PO_4 -based composites have been prepared, including metal oxides/ Ag_3PO_4 ,^{15,16} composite oxides/ Ag_3PO_4 ,^{17,18} carbon materials / Ag_3PO_4 ,¹⁹⁻²¹ plasmonic catalysts / Ag_3PO_4 ,^{22, 23} etc.

Inspired by the excellent properties of graphene, two dimensional graphene-like materials have attracted considerable attention because they exhibited many appealing properties for a wide range of applications, such as catalysis, light harvesting, batteries.²⁴⁻²⁶ Graphene-like hexagonal boron nitride (h-BN) as a graphene analogue, is a wide band gap material with a lattice constant similar to graphene, and has very high mechanical strength, good thermal conductivity, excellent chemical and thermal stability.²⁷ As a result, h-BN has a wide range of applications, such as deep ultraviolet light emitters, transparent membranes, protective coatings, and dielectric layers.²⁸ Recently, after introduction of h-BN, it would improve the photocatalytic performance of the bulk semiconductors.²⁹⁻³² In the presence of the h-BN, it promoted the separation of electrons and holes in the photocatalytic reaction. Therefore, h-BN can act as an supporting matrix and a metal-free co-material. In order to broaden the application areas of graphene-like BN, it is necessary to design new graphene-like BN composites photocatalyst. Compared with the graphene or graphene oxide, it was worth to further analyze the role of graphene-like BN in the photocatalysis.

In this work , the object was to exploration of new graphene-like photocatalysts.

Herein, a new photocatalyst based on Ag_3PO_4 and graphene-like BN was designed to attain the efficient degradation of pollutants under visible light irradiation. The role of graphene-like BN in the enhancing photocatalytic performance was investigated based on the characterization and the photocatalytic degradation experiment. The kinetics and possible photocatalytic mechanism of graphene-analogue $\text{BN}/\text{Ag}_3\text{PO}_4$ were also discussed.

2. Experimental section

2.1 Synthesis of graphene-analogues BN

The graphene-analogues BN were synthesized by a chemical method.³³ In a typical synthesis run, boric acid and urea mixtures with 1:24 were dissolved in 40 mL of and heated at 65°C. The dried mixtures were heated at 900°C for 5 h in a N_2 atmosphere, then the white BN products were obtained.

2.2 Synthesis of graphene-analogue $\text{BN}/\text{Ag}_3\text{PO}_4$ photocatalysts

The typical preparation procedure of the graphene-analogue $\text{BN}/\text{Ag}_3\text{PO}_4$ photocatalysts was as follows: 0.004 g of the graphene-analogue BN was added into 30 mL of distilled water and sonicated for 30 min. Then, 0.34 g AgNO_3 was added into the above suspension and stirred for 15 min. Further, 20 mL of 0.03 M Na_3PO_4 was added drop by drop under stirring, and the mixture was held in the dark for 60 min with continuous stirring. The obtained precipitate was collected by centrifugation and washed with distilled water for three times. Finally, the solid product was dried at 50°C for 6 h. In this way, different graphene-analogue $\text{BN}/\text{Ag}_3\text{PO}_4$ photocatalysts (wt% = 0.1, 1, 5) were obtained, respectively. The synthesis process could be seen as

illustrated in Fig. 1.

2.3 Characterization of photocatalyst

X-ray diffraction patterns (XRD) of the samples recorded at room temperature, by a Bruker D8 advance X-ray diffractometer using Cu K α radiation. Transmission electron microscopy (TEM) micrographs were taken with a JEOL-JEM-2010(JEOL, Japan) operated at 200 kV. Scanning electron microscopy (SEM) images of the sample were taken on a field emission scanning electron microscope (JEOL JSM-7001F). The chemical composition of the samples was determined by EDS. UV-visible absorbance spectra were obtained by a UV-visible spectrophotometer (DRS, Shimadzu UV-2450, Japan). The structural information of samples was measured by a Fourier transform spectrophotometer (FT-IR, Nicolet Model Nexus 470) using the standard KBr disk method. The X-ray photoelectron spectroscopy (XPS) measurements were performed on an ESCALab MKII X-ray photo-electron spectrometer using Mg-K α radiation.

2.4 Photocatalytic activity test

The photocatalytic performance of graphene-analogue BN/Ag₃PO₄ composites was evaluated using the degradation of RhB degradation as a probe reaction under visible light irradiation. A 300 W Xe lamp with a 400 nm cutoff filter was used as the light source. In a typical photodegradation process, 75 mg photocatalyst was dispersed in 75 mL of RhB aqueous solution with an initial concentration of 10 mg L⁻¹. Prior to the light irradiation, the dispersion was kept in the dark for 30 min under magnetic stirring to reach the adsorption-desorption equilibrium. After the photodegradation,

the photocatalysts were separated from the reaction solutions by centrifugation and the concentration of RhB (553 nm) was determined by UV-vis spectrophotometer.

3. Results and discussion

3.1 Crystal pattern analysis

Fig. 2 shows the XRD patterns of graphene-analogue BN, Ag_3PO_4 and graphene-analogue BN/ Ag_3PO_4 . The XRD pattern of graphene-analogue BN displayed broaden peaks located at around 25.5° and 42.6° , which indicated that the graphene-analogue BN had hexagonal structure.³⁴ For the graphene-analogue BN/ Ag_3PO_4 composites, it could be clearly seen that all the diffraction peaks of the composites corresponded to the body-centered cubic structure of Ag_3PO_4 (JCPDS no 06-0505). These phases could be characterised by the appearance of Bragg diffraction peaks at $2\theta = 20.9^\circ, 29.7^\circ, 33.3^\circ, 36.6^\circ, 42.5^\circ, 47.8^\circ, 52.7^\circ, 55.0^\circ, 57.3^\circ, 61.6^\circ, 65.8^\circ, 69.9^\circ, 72.0^\circ$ and 73.9° were indexed to (110), (200), (210), (211), (220), (310), (222), (320), (321), (400), (330), (420), (421) and (332) planes for Ag_3PO_4 , respectively.³⁵ However, no diffraction peaks of graphene-analogue BN were observed when BN loading amount was from 0.1 wt.% to 5 wt.%. When graphene-analogue BN amount was 10 wt.%, the weak diffraction peak of graphene-analogue BN (located at $2\theta = 25.5^\circ$) could be detected. Besides, no other diffraction peaks could be observed in the pattern.

3.2 XPS analysis

To further confirm the co-existence of graphene-analogue BN and Ag_3PO_4 in the composites, XPS analysis has also been performed. As shown in Fig. 3A, it can be clearly observed that except for the Ag, P, and O elements coming from Ag_3PO_4 , the

B and N elements corresponding to the BN have also been detected. The appearance of C 1s peak (284.8 eV) is mainly due to the adventitious hydrocarbon from the XPS instrument itself (Fig. 3 B). For Ag 3d (Fig. 3C), two peaks are observed at binding energies of about 368.0 and 374.0 eV, corresponding to Ag 3d_{5/2} and Ag 3d_{3/2}, respectively.³⁶ In Fig. 3D, the P 2p peak of the material appears at 132.4 eV, which corresponded to P⁵⁺ according to the previous reports.³⁷ From Fig. 3E, it can be seen that the binding energy of XPS spectra of O 1s is 530.7 eV, corresponding to oxygen in the sample lattice.³⁸ Compared with the C1s, P 2p and O1s of the pure Ag₃PO₄, it could be seen that the XPS peak of C 1s(284.8 eV), P 2p(132.4 eV) and O1s(530.7 eV) in the BN/Ag₃PO₄ composite did not change. High-resolution XPS spectra of B 1s and N 1s are shown in Fig. 3F and 3G. The peak at 190.1 eV in B 1s spectra was assigned to B-N bonds.³⁹ The N 1s core-level XPS spectrum shows a strong photoelectron signal at 398.3 eV, which is in agreement with literature values for N³⁻ in BN.⁴⁰

3.3 SEM and TEM analyses

In order to further show the morphology and microstructure of the graphene-analogue BN/Ag₃PO₄ with different BN contents, the SEM and TEM of all the samples were given, as shown a in Fig. 4 and 5. In the SEM analysis (Fig. 4A), it could be found that the pure Ag₃PO₄ has irregular nanoparticle morphology and relatively smooth surface. Fig. 4B-E indicated that the Ag₃PO₄ nanoparticles were wrapped and supported by graphene-analogue BN, just like the graphene-based materials.^{41, 42} It is found that the graphene-analogue BN looks highly transparent with silky wavy like appearance (Fig. 4F). The detailed structural information about the graphene-analogue BN/Ag₃PO₄ samples was further investigated by TEM (Fig. 5). In

Fig. 5A, the size of Ag_3PO_4 particles was estimated about between 80 and 200 nm. A part of the Ag_3PO_4 material formed aggregation, and composed of larger size particles. Fig. 5 B-E shows typical TEM images of the representative graphene-analogue $\text{BN}/\text{Ag}_3\text{PO}_4$ samples with different BN contents. It could be found that Ag_3PO_4 particles anchoring on the surface of graphene-analogue BN. The Ag_3PO_4 particles were dispersed on the surface of graphene-analogue BN and a heterojunction structure might be formed. In order to confirm the heterostructure between the graphene-analogue BN and Ag_3PO_4 nanoparticles, the experiment had also investigated the samples by HRTEM. However, the Ag_3PO_4 particles were destroyed by the high-energy electron beam during the measurement, and the morphology of the samples was distorted. That was the reason why the HRTEM of Ag_3PO_4 could get hardly, and similar result had been reported by Bi and Cao et al.^{43,44}

3.4 FT-IR analysis

Fig. 6 shows the typical FT-IR spectrum of the graphene-analogue $\text{BN}/\text{Ag}_3\text{PO}_4$ composites. It was found that all the graphene-analogue $\text{BN}/\text{Ag}_3\text{PO}_4$ have similar FT-IR peaks at 1015 cm^{-1} and 550 cm^{-1} , which are correspond to the symmetric stretching vibration mode of the PO_4^{3-} group.⁴⁵ For the pure BN, the FT-IR spectrum of h-BN alone contains two characteristic absorption bands at 1378 cm^{-1} and 805 cm^{-1} , which correspond to the in-plane B-N stretching mode and the plane B-N-B bending mode, respectively.^{46, 47} In the case of the graphene-analogue $\text{BN}/\text{Ag}_3\text{PO}_4$ samples, the typical absorption peaks of BN was also observed at 1378 cm^{-1} . However, the stretching vibration of the B-N-B at 805 cm^{-1} had shifted to the higher wavenumber (870 cm^{-1}). It was found that the IR peak at 805 cm^{-1} became hindered due to

introduction of Ag_3PO_4 in the sample and also in the $\text{BN}/\text{Ag}_3\text{PO}_4$ hybrids shifting it to higher frequency (870 cm^{-1}). Generally, introduction of the hybrid material to graphene material could cause offset of IR absorption peaks.^{48,49} Therefore, this indicated a possibility of compounding between BN and Ag_3PO_4 . All the results indicated that Ag_3PO_4 nanoparticles were successfully supported on or hybridized with graphene-analogue BN.

3.5 DRS analysis

The optical absorption properties play an important role in determining the photocatalytic activity of the samples. The optical properties of graphene-analogue BN and graphene-analogue $\text{BN}/\text{Ag}_3\text{PO}_4$ composites were investigated by UV-vis diffuse reflectance spectra, as shown in Fig.7. It could be seen that the pure Ag_3PO_4 presented strong absorption from the UV light to approximately 500 nm. Meanwhile, the absorption of BN was threshold at 310 nm. Therefore, the band gap of h-BN could be calculated to be ca. 4.0 eV. The literature had reported that the band gap of BN was found between 3.9 eV and 5.9 eV.²⁹ Compared with the pure Ag_3PO_4 , all of the graphene-analogue $\text{BN}/\text{Ag}_3\text{PO}_4$ composites displayed continuous strong absorption in the range of 500-800 nm. With the increasing BN contents in graphene-analogue $\text{BN}/\text{Ag}_3\text{PO}_4$ composites, the sample color gradually changed and the absorption intensity of the composites was also increased. This enhancement would also have effected on the separation of the photo-generated carriers,⁵⁰ leading to higher photocatalytic activity. A similar result has also been reported by Chen et al.³²

3.6 Photocatalytic activity and stability of of the samples

In this work, RhB solution was used as a model pollutant for the evaluation of photocatalytic activity of the graphene-analogue $\text{BN}/\text{Ag}_3\text{PO}_4$ composites. The photocatalytic activity of the samples was shown in Fig. 8A. After irradiation for 12

min, 70% of RhB was degraded by pure Ag_3PO_4 nanoparticles. However, after adding a little amount of graphene-analogue BN (≤ 0.5 wt.%), the photocatalytic activity of graphene-analogue BN/ Ag_3PO_4 composites was remarkably enhanced. When the graphene-analogue BN content gradually changed from 0.1 to 0.5 wt.%, the photocatalytic degradation efficiency of RhB were greatly improved correspondingly, and about 97% of RhB has been degraded. However, a further increasing in BN content (> 0.5 wt.%) could lead to decrease of the photocatalytic activity. Especially for the sample with a content of 5 wt.%, it shows a drastic decrease in photocatalytic activity. Thus, under visible light illumination the optimum BN content was 0.5 wt.%. The further increase of the BN content led to a deterioration of the photocatalytic performance, because of the “shielding effect”.⁵¹ That is to say, the higher addition ratio of BN into the composite would be decrease the contact surface of Ag_3PO_4 nanoparticles with the light irradiation, which would lead to a decreased photocatalytic activity.⁵¹ Compared with graphene oxide/ Ag_3PO_4 (6%, optimal GO content),⁵² graphene-analogue BN/ Ag_3PO_4 (0.5%, optimal BN content) has the similar photocatalytic degradation efficiency. Compared with the previous literature, like graphene, in the presence of the graphene-analogue BN, it can effectively enhance the photocatalytic activity and stability of the Ag_3PO_4 material.⁵³⁻⁵⁵ Therefore, it is significant for using graphene-like BN instead of GO with high efficient photocatalytic activity. In addition, the photocatalytic activity of the as-prepared graphene-analogues BN/ Ag_3PO_4 composite was also evaluated by the degradation of methylene blue (MB) and 4-chlorophenol (4-CP) under the same condition. From Fig. 8B, it can be seen that about 93% of MB has been degraded after 12 min irradiation by graphene-analogues BN/ Ag_3PO_4 (0.5 wt.%) and only 80% of MB has been degraded by the pure Ag_3PO_4 (Fig. 8B). As shown in Fig. 8C, it could be found that

after 30 min irradiation, no degradation of 4-CP was observed in the direct photolysis, and 44% and 61% of 4-CP was degraded in the case of Ag_3PO_4 and $\text{BN}/\text{Ag}_3\text{PO}_4(0.5 \text{ wt.}\%)$ samples, respectively, indicating that the $\text{BN}/\text{Ag}_3\text{PO}_4(0.5 \text{ wt.}\%)$ material were efficient visible-light-driven photocatalysts. This demonstrated the superiority of the as-prepared graphene-analogues $\text{BN}/\text{Ag}_3\text{PO}_4$ composite.

The photocatalyst of Degussa P25(TiO_2) and graphene-analogues $\text{BN}/\text{P25}(0.5 \text{ wt.}\%)$ were also respectively used as comparison to decompose RhB under the same condition. Fig. 8D displays the degradation of RhB over different photocatalysts under visible light irradiation. It could be seen that P25 and graphene-analogues $\text{BN}/\text{P25}(0.5 \text{ wt.}\%)$ were almost no photocatalytic activity after 12 min irradiation. However, under the same irradiation conditions, the photocatalytic degradation efficiency of graphene-analogues $\text{BN}/\text{Ag}_3\text{PO}_4 (0.5 \text{ wt.}\%)$ can arrived 97%.

Considering the influence of the reaction temperatures on the photocatalytic activity, it had added the experiments on the sample with 0.5 wt% at different photocatalytic reaction temperatures (20°C , 25°C , 30°C). Fig.8E displays the photocatalytic degradation of RhB over different temperatures under visible light irradiation. After irradiation for 12 min, 50% of RhB was degraded when the temperature was 20°C . However, after increasing the reaction temperature, the photocatalytic activity of graphene-analogue $\text{BN}/\text{Ag}_3\text{PO}_4 (0.5 \text{ wt.}\%)$ composites was remarkably enhanced. When the temperature increased to 30°C , the photocatalytic degradation efficiency was 97% after irradiation for 12 min. The high reaction temperature is beneficial to enhance the photocatalytic activity.

Besides, the interaction between BN and Ag_3PO_4 in the composites still could be confirmed through a series of photocatalytic activity experiments. The

graphene-analogue BN/Ag₃PO₄(0.5 wt.%) heterojunction had higher photocatalytic activity than mathematical sum of BN and Ag₃PO₄. The content of each component in the photocatalyst was the same as in BN/Ag₃PO₄(0.5 wt.%), but the photocatalytic degradation efficiency of RhB was 70% and 97%, respectively. It was significantly proved that there were interaction between graphene-analogue BN and Ag₃PO₄ in the composites, and the heterojunction structure might be formed between the graphene-analogue BN and Ag₃PO₄ in the composites. In conclusion, all the above analyses and experiments had proved that BN had interacted with Ag₃PO₄ and the heterojunction between BN and Ag₃PO₄ might be formed.

It also defined that the photocatalytic reaction followed a pseudo-first-order reaction for low concentration of the dye solutions, the relevant equations are listed as follows: $-\ln(C/C_0) = kt$, where C_0 and C are the concentrations of reactant at time 0 and t , respectively, and k is the first-order reaction rate constant. It was found that the rate constant k for RhB degradation increased firstly, and then dramatically decreased with the increasing of the content of BN in the composites, as shown in Fig. 9. The graphene-analogue BN/Ag₃PO₄ composites exhibited the maximum k (0.28 min⁻¹), which was three times than that of the pure Ag₃PO₄ (0.08 min⁻¹). The kinetic constants and relative coefficient over the photocatalysts could be seen in Table 1. In a word, the graphene-analogue BN/Ag₃PO₄ composite photocatalyst had notably enhanced activity in photocatalytic degradation of RhB. These results suggested a synergistic effect between the BN sheet and Ag₃PO₄ nanoparticles.

As shown in Fig. 10, the absorption of RhB at 553 nm significantly decreased with

increasing irradiation time. It was also found that the maximum absorption wavelength did not exhibit blue shift or red shift. In the meantime, no new absorption appears in either the visible or ultraviolet region, which indicated the complete photocatalytic mineralization of dye during the photocatalytic reaction.

The stability of the photocatalyst was important for its application. To investigate the potential application under visible light irradiation, the graphene-analogue BN/Ag₃PO₄(0.5 wt.%) was used to degrade RhB dye in five repeated cycles, and the experimental results are shown in Fig. 11. It was found that the photocatalytic degradation efficiency of the graphene-analogue BN/Ag₃PO₄(0.5 wt.%) still reached 94%, even though it had been used five times, indicating graphene-analogue BN/Ag₃PO₄ was highly stable. In the previous reports, many researchers indicated that Ag₃PO₄ was unstable and could be easily decomposed under the visible light irradiation.^{10,56} Therefore, in the presence of the BN, the stability of composite improved. The corresponding XRD pattern of the used sample after the RhB degradation experiments found that there is no change in position and intensity of all the diffraction peaks and there are no other phases detected in the XRD patterns of the photocatalyst.

3.7 Photocurrent analysis

Fig. 12 shows the transient photocurrent responses via five on-off cycles of pure Ag₃PO₄ and graphene-analogue BN/Ag₃PO₄ electrodes under visible light irradiation. the photocurrent of the graphene-analogue BN/Ag₃PO₄ (0.5 wt.%) was about 1.4 times as high as that of the pure Ag₃PO₄ sample, indicating that the separation and

transfer of photoinduced electron-hole pairs were more efficient in the case of the graphene-analogue BN/Ag₃PO₄ sample due to the interfacial interaction between BN and Ag₃PO₄.⁵⁷

3.8 Photocatalytic mechanisms

Radical and hole trapping experiments were used to detect the main oxidative species in the photocatalytic reaction process. As is shown in Fig. 13, it could be seen that the photocatalytic activity had a little change after adding the scavenger of radicals (*t*-BuOH). However, the photodegradation efficiency of RhB was greatly inhibited when a hole scavenger, EDTA-2Na, was added into the photocatalytic reaction. This results indicated that the degradation of RhB was achieved by direct hole oxidation in the composite. In principle, specific surface was a crucial factor for photocatalytic activity. The BET surface areas of the pure Ag₃PO₄, BN/Ag₃PO₄(0.1 wt.%), BN/Ag₃PO₄(0.5 wt.%), BN/Ag₃PO₄(1 wt.%) and BN/Ag₃PO₄(5 wt.%) were evaluated to be about 2.9 m² g⁻¹, 6.2 m² g⁻¹, 7.6 m² g⁻¹, 8.2 m² g⁻¹ and 10.3 m² g⁻¹, respectively. It was clear that the BET surface areas of the samples were slightly improved with the increasement of BN content. Therefore, in the case of the BN-Ag₃PO₄ system, due to the increasing surface area of the composites, the more organic pollutant molecules adsorbed in the surface of the BN. Under the visible light irradiation, the photon-generated electron and hole pairs of the Ag₃PO₄ could be separated, and the electrons at the valence band (VB) could be excited to the conduction band (CB). In the presence of the BN, it was to suppress the recombination of photogenerated electron and holes. The improved charge separation ability should be ascribed to the surface negatively charged BN or BN could be used

as a surface passivation material to modify the surface/interface photogenerated electron behavior of photocatalysts, which had been confirmed by the literature in other groups.^{29,30} So, the photon-generated holes in the Ag_3PO_4 nanoparticles quickly participate in the photocatalytic degradation of the organic pollutants which had been adsorbed on the surface of the BN. Therefore, the high photocatalytic activity of the the graphene-analogue BN/ Ag_3PO_4 composite could be due to the synergetic role between graphene-analogue BN and Ag_3PO_4 . The detailed photocatalytic mechanism in improved photocatalytic activity of graphene-analogue BN/ Ag_3PO_4 was illustrated in Fig. 14.

4. Conclusions

In summary, the graphene-analogue BN/ Ag_3PO_4 samples showed higher photocatalytic activity than the pure Ag_3PO_4 , and the optimal loading BN contents were 0.5 wt% . The photocatalytic degradation of RhB over the samples obeyed pseudo-first-order kinetics, and the photocatalytic degradation rate by the graphene-analogue BN/ Ag_3PO_4 composite (0.5 wt.%) was about three times than that of the pure Ag_3PO_4 . In the presence of the graphene-analogue BN, it was to suppress the recombination of photogenerated electron and holes. The improved charge separation ability could be ascribed to the surface negatively charged BN or BN could be used as a surface passivation material to modify the surface/interface photogenerated electron behavior of photocatalysts.

Acknowledgements

The work was supported by National Nature Science Foundation of China (21476097, 21476098, 21406094), Natural Science Foundation of Jiangsu Province

(BK20140533), Postdoctoral Foundation of China (2014M551520), Doctoral Innovation Doctoral Innovation Fund of Jiangsu (CXLX13-651) and Opening Project (no. SJHG1308) of the Jiangsu Key Laboratory for Environment Functional Materials.

References

- 1 L. Jing, W. Zhou, G. Tian and H. Fu, *Chem. Soc. Rev.*, 2013, **42**, 9509-9549.
- 2 Q. Xiang, J. Yu and M. Jaroniec, *Chem. Soc. Rev.*, 2012, **41**, 782-796.
- 3 P. Zhou, J. Yu and M. Jaroniec, *Adv. Mater.*, 2014, **29**, 4920-4935.
- 4 Y. Qu and X. Duan, *Chem. Soc. Rev.*, 2013, **42**, 2568-2580.
- 5 H. Zhang, X. Fan, X. Quan, S. Chen and H. Yu, *Environ. Sci. Technol.*, 2011, **45**, 5731-5736.
- 6 P. Zhang, J. Zhang and J. Gong, *Chem. Soc. Rev.*, 2014, **43**, 4395-4422.
- 7 J. Tian, Y. Sang, G. Yu, H. Jiang, X. Mu and H. Liu, *Adv. Mater.*, 2013, **36**, 5075-5080.
- 8 Y. Bi, S. Ouyang, N. Umezawa, J. Cao and J. Ye, *J. Am. Chem. Soc.*, 2011, **133**, 6490-6492.
- 9 Z. Yi, J. Ye, N. Kikugawa, T. Kako, S. Ouyang, H. Stuart-Williams, H. Yang, J. Cao, W. Luo, Z. Li, Y. Liu and R. L. Withers, *Nat. Mater.*, 2010, **9**, 559-564.
- 10 H. Wang, Y. Bai, J. Yang, X. Lang, J. Li and L. Guo, *Chem. Eur. J.*, 2012, **18**, 5524-5529.
- 11 H. Hu, Z. Jiao, H. Yu, G. Lu, J. Ye and Y. Bi, *J. Mater. Chem. A.*, 2013, **1**, 2387-2390.
- 12 Z. Jiao, Y. Zhang, H. Yu, G. Lu, J. Ye and Y. Bi, *Chem Commun*, 2013, **49**, 636-638.
- 13 Y. Bi, H. Hu, S. Ouyang, G. Lu, J. Cao and J. Ye, *Chem Commun*, 2012, **48**, 3748-3750.
- 14 G. Huang, Z. Ma, W. Huang, Y. Tian, C. Jiao, Z. Yang, Z. Wan and A. Pan, *J. Nanomater.*, 2013, 71356.
- 15 J. Zhang, K. Yu, Y. Yu, L. Lou, Z. Yang, J. Yang and S. Liu, *J. Mol. Catal. A: Chem.*, 2014, **391**, 12-18.
- 16 Z. Yang, G. Huang, W. Huang, J. Wei, X. Yan, Y. Liu, C. Jiao, Z. Wan and A. Pan, *J. Mater. Chem. A.*, 2014, **2**, 1750-1756.
- 17 J. Guo, S. Ouyang, P. Li, Y. Zhang, T. Kako and J. Ye, *Appl. Catal. B*, 2013, **134**, 286-292.
- 18 H. Lin, H. Ye, B. Xu, J. Cao and S. Chen, *Catal. Commun.*, 2013, **37**, 55-59.

- 19 Q. Xiang, D. Lang, T. Shen and F. Liu, *Appl. Catal., B*, 2015, **162**, 196-203.
- 20 H. Xu, C. Wang, Y. Song, J. Zhu, Y. Xu, J. Yan, Y. Song and H. Li, *Chem. Eng. J.*, 2014, **241**, 35-42.
- 21 X. Yang, H. Cui, Y. Li, J. Qin, R. Zhang and H. Tang, *ACS Catal.*, 2013, **3**, 363-369.
- 22 M. Gondal, X. Chang, W. Sha, Z. Yamani and Q. Zhou, *J. Colloid Interface Sci.*, 2013, **392**, 325-330.
- 23 Y. Liu, L. Fang, H. Lu, Y. Li, C. Hu and H. Yu, *Appl. Catal. B*, 2012, **115-116**, 245-252.
- 24 M. Xu, T. Liang, M. Shi and H. Chen, *Chem. Rev.*, 2013, **113**, 3766-3798.
- 25 X. Huang, Z. Zeng and H. Zhang, *Chem. Soc. Rev.*, 2013, **42**, 1934-1946.
- 26 M. Chhowalla, H. S. Shin, G. Eda, L. Li, K. P. Loh and H. Zhang, *Nat. Chem.*, 2013, **5**, 263-275.
- 27 Y. Gao, W. Ren, T. Ma, Z. Liu, Y. Zhang, W. B. Liu, L. P. Ma, X. Ma and H. M. Cheng, *ACS Nano*, 2013, **7**, 5199-5206.
- 28 S. Z. Butler, S. M. Hollen, L. Cao, Y. Cui, J. A. Gupta, H. R. Gutierrez, T. F. Heinz, S. S. Hong, J. Huang, A. F. Ismach, E. Johnston-Halperin, M. Kuno, V. V. Plashnitsa, R. D. Robinson, R. S. Ruoff, S. Salahuddin, J. Shan, L. Shi, M. G. Spencer, M. Terrones, W. Windl and J. E. Goldberger, *ACS Nano*, 2013, **7**, 2898-2926.
- 29 X. Fu, Y. Hu, Y. Yang, W. Liu and S. Chen, *J. Hazard. Mater.*, 2013, **244-245**, 102-110
- 30 X. Fu, Y. Hu, T. Zhang and S. Chen, *Appl. Surf. Sci.*, 2013, **280**, 828-835.
- 31 C. Tang, J. Li, Y. Bando, C. Zhi and D. Golberg, *Chem. Asian J.*, 2010, **5**, 1220-1224.
- 32 D. Liu, W. Cui, J. Lin, Y. Xue, Y. Huang, J. Li, J. Zhang, Z. Liu and C. Tang, *Catal. Commun.*, 2014, **57**, 9-13.
- 33 A. Nag, K. Raidongia, K. P. S. S. Hembaram, R. Datta, U. V. Waghmare and C. N. R. Rao, *ACS Nano*, 2010, **4**, 1539-1544.

- 34 M. Wang, M. Li, L. Xu, L. Wang, Z. Ju, G. Li and Y. Qian, *Catal. Sci. Technol.*, 2011, **1**, 1159-1165.
- 35 Y. Wang, X. Li, Y. Wang, C. Fan, *J. Solid State Chem.*, 2013, **202**, 51-56.
- 36 W. Liu, M. Wang, C. Xu, S. Chen and X. Fu, *Mater. Res. Bull.*, 2013, **48**, 106-113.
- 37 H. Yu, Q. Dong, Z. Jiao, T. Wang, J. Ma, G. Lu and Y. Bi, *J. Mater. Chem. A*, 2014, **2**, 1668-1671.
- 38 R. Y. Zheng, L. Lin, J. L. Xie, Y. Z. Zhu and Y. C. Xie, *J. Phys. Chem. C*, 2008, **112**, 15502-15509.
- 39 W. Lei, D. Portehault, D. Liu, S. Qin and Y. Chen, *Nat. Commun.*, 2013, 1777.
- 40 C. Huang, W. Ye, Q. Liu and X. Qiu, *ACS Appl. Mater. Interfaces*, DOI: 10.1021/am5037737
- 41 H. Huang, Y. Huang, M. Wang, X. Chen, Y. Zhao, K. Wang and H. Wu, *Electrochim. Acta*, 2014, **147**, 201-208.
- 42 L. Ye and Z. Li, *Appl. Catal. B*, 2014, **160–161**, 552–557
- 43 Y.P. Bi, S.X. Ouyang, J.Y. Cao and J.H. Ye, *Phys. Chem. Chem. Phys.*, 2011, **13**, 10071-10075.
- 44 J. Cao, B.D. Luo, H.L. Lin, B.Y. Xu, S.F. Chen, *J. Hazard. Mater.*, 2012, **217-218**, 107-115.
- 45 C. Cui, Y. Wang, D. Liang, W. Cui, H. Hu, B. Lu, S. Xu, X. Li, C. Wang and Y. Yang, *Appl. Catal. B*, 2014, **158–159**, 150–160.
- 46 M. Wang, M. Li, L. Xu, L. Wang, Z. Ju, G. Li and Y. Qian, *Catal. Sci. Technol.*, 2011, **1**, 1159-1165.
- 47 J. Chen, J. Zhu, Z. Da, H. Xu, J. Yan, H. Ji, H. Shu, H. Li, *Appl. Surf. Sci.*, 2014, **313**, 1-9.
- 48 X. Wang, C. Qing, Q. Zhang, W. Fan, X. Huang, B. Yang and J. Cui, *Electrochim. Acta*, 2014,

134, 371-376.

49 P. Routh, R. K. Layek and A.K. Nandi, *Carbon*, 2012, **50**, 3422-3434.

50 E. Gao and W. Wang, *Nanoscale*, 2013, **5**, 11248-11256.

51 Y. Zhang, Z. R.Tang, X. Fu and Y. J. Xu, *ACS Nano*, 2010, **4**, 7303-7314.

52 C. Wang, J. Zhu, X. Wu, H. Xu, Y. Song, J. Yan, Y. Song, H. Ji, K. Wang and H. Li, *Ceram. Int.*, 2014, **40**, 8061-8070.

53 L. Liu, J. Liu and D. D. Sun, *Catal. Sci. Technol.*, 2012, **2**, 2525-2532

54 Y. Ao, P. Wang, C. Wang, J. Hou and J. Qian, *Appl. Surf. Sci.*, 2013, **271**, 265-270.

55 G. Chen, M. Sun, Q. Wei, Y. Zhang, B. Zhu and B. Du, *J. Hazard. Mater.*, 2013, **244-245**, 86-93

56 P. Dong, Y. Wang, B. Cao, S. Xin, L. Guo, J. Zhang, F. Li, *Appl. Catal. B*, 2013, **132-133**, 45-53.

57 X. Bai, L. Wang and Y. Zhu, *ACS Catal.*, 2012, **2**, 2769-2778.

Table 1. Kinetic Constants (k) and relative coefficient (R) for the degradation of RhB under visible light irradiation.

photocatalysts	$k(\text{min}^{-1})$	R^2
Pure Ag_3PO_4	0.08	0.98
BN/ Ag_3PO_4 (0.1 wt%)	0.11	0.98
BN/ Ag_3PO_4 (0.5 wt%)	0.28	0.99
BN/ Ag_3PO_4 (1 wt%)	0.06	0.98
BN/ Ag_3PO_4 (5 wt%)	0.02	0.98

Figure Captions

Fig. 1 Schematic illustration of the fabrication of graphene-analogue BN/Ag₃PO₄ photocatalysts.

Fig. 2 XRD patterns of the prepared BN, Ag₃PO₄ and graphene-analogue BN/Ag₃PO₄ composites.

Fig. 3 XPS spectra of (A) BN/Ag₃PO₄, (B) C 1S, (C) Ag 3d, (D) P 2p, (E) O 1S, (F) B 1s, (G) N 1s.

Fig. 4 SEM images of (A) pure Ag₃PO₄, (B) graphene-analogue BN/Ag₃PO₄(0.1 wt.%), (C) graphene-analogue BN/Ag₃PO₄(0.5 wt.%), (D) graphene-analogue BN/Ag₃PO₄ (1 wt.%), (E) graphene-analogue BN/Ag₃PO₄ (5 wt.%), (F) graphene-analogue BN.

Fig. 5 TEM images of (A) pure Ag₃PO₄, (B) graphene-analogue BN/Ag₃PO₄(0.1 wt.%), (C) graphene-analogue BN/Ag₃PO₄(0.5 wt.%), (D) graphene-analogue BN/Ag₃PO₄(1 wt.%), (E) graphene-analogue BN/Ag₃PO₄ (5 wt.%), (F) graphene-analogue BN.

Fig. 6 FT-IR spectra of the graphene-analogue BN/Ag₃PO₄ composites.

Fig. 7 UV-Vis absorption spectra of BN, Ag₃PO₄, and the graphene-analogue BN/Ag₃PO₄ composites with various BN contents.

Fig. 8 Photocatalytic efficiency in the case of Ag₃PO₄ and BN/Ag₃PO₄ for (A) RhB degradation, (B) MB degradation, (C) 4-CP degradation under visible light irradiation; (D) Compared the photocatalytic activity with other materials(for RhB degradation), (E) Photocatalytic degradation efficiency of RhB at different reaction temperature.

Fig. 9 First-order kinetics data for the photodegradation of RhB over Ag₃PO₄ and BN/Ag₃PO₄ samples.

Fig. 10 Absorption spectra of RhB after different irradiation times in the presence of graphene-analogue BN/Ag₃PO₄(0.5 wt.%).

Fig. 11 Cycling runs for photocatalytic degradation of RhB over graphene-analogue BN/Ag₃PO₄ composite (0.5 wt.%).

Fig. 12 Photocurrent responses of Ag₃PO₄ and graphene-analogue BN/Ag₃PO₄.

Fig. 13 Photocatalytic degradation experiments with the addition of hole and radical scavenger.

Fig. 14 The proposed photocatalytic mechanism of graphene-analogue BN/Ag₃PO₄ composite.

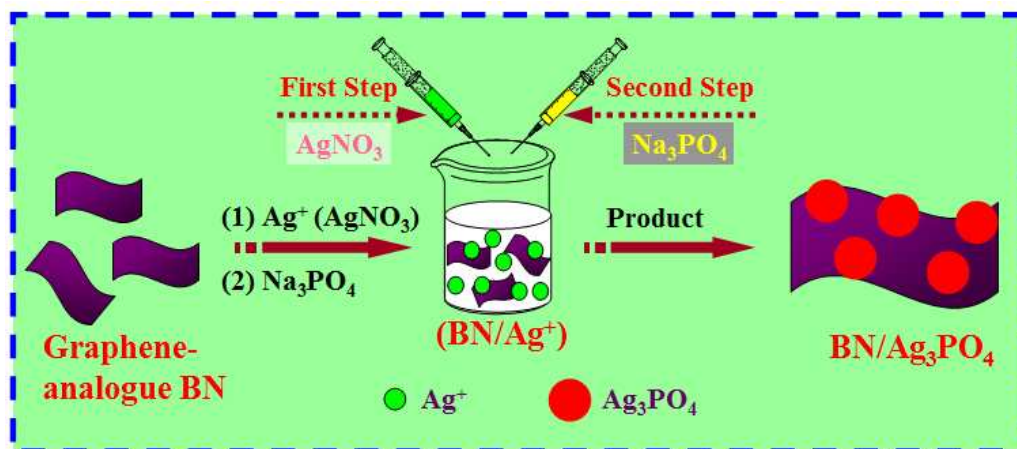


Fig. 1 Schematic illustration of the fabrication of graphene-analogue BN/Ag₃PO₄ photocatalysts.

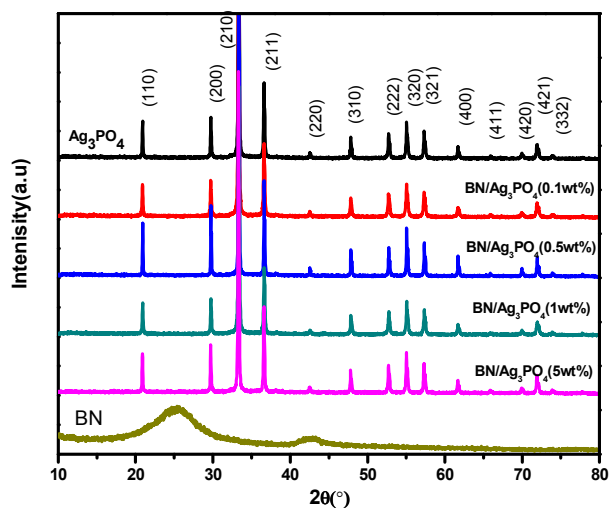


Fig. 2 XRD patterns of the prepared BN, Ag₃PO₄ and graphene-analogue BN/Ag₃PO₄ composites.

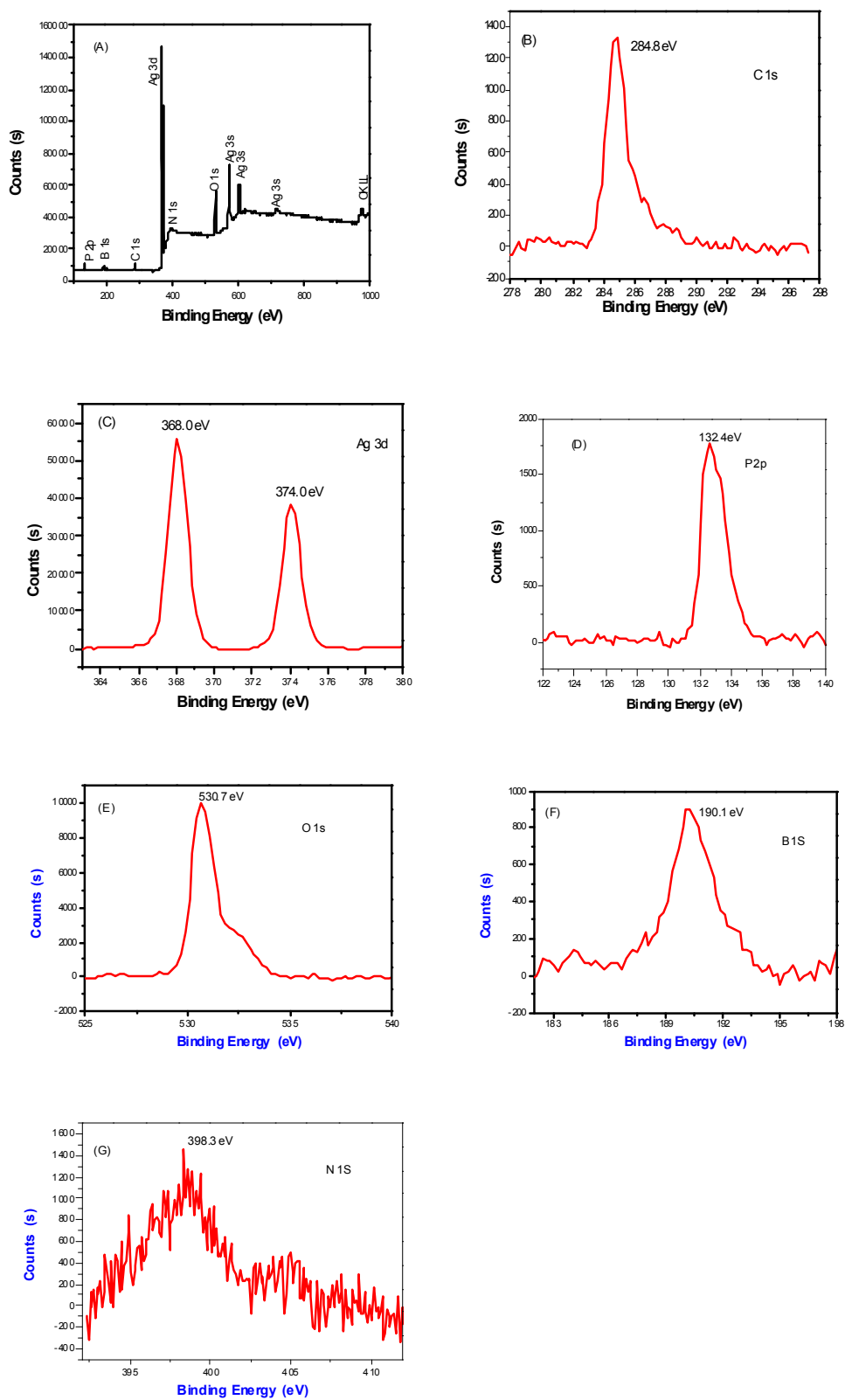


Fig. 3 XPS spectra of (A) BN/Ag₃PO₄, (B) C 1s, (C) Ag 3d, (D) P 2p, (E) O 1s, (F) B 1s, (G) N 1s.

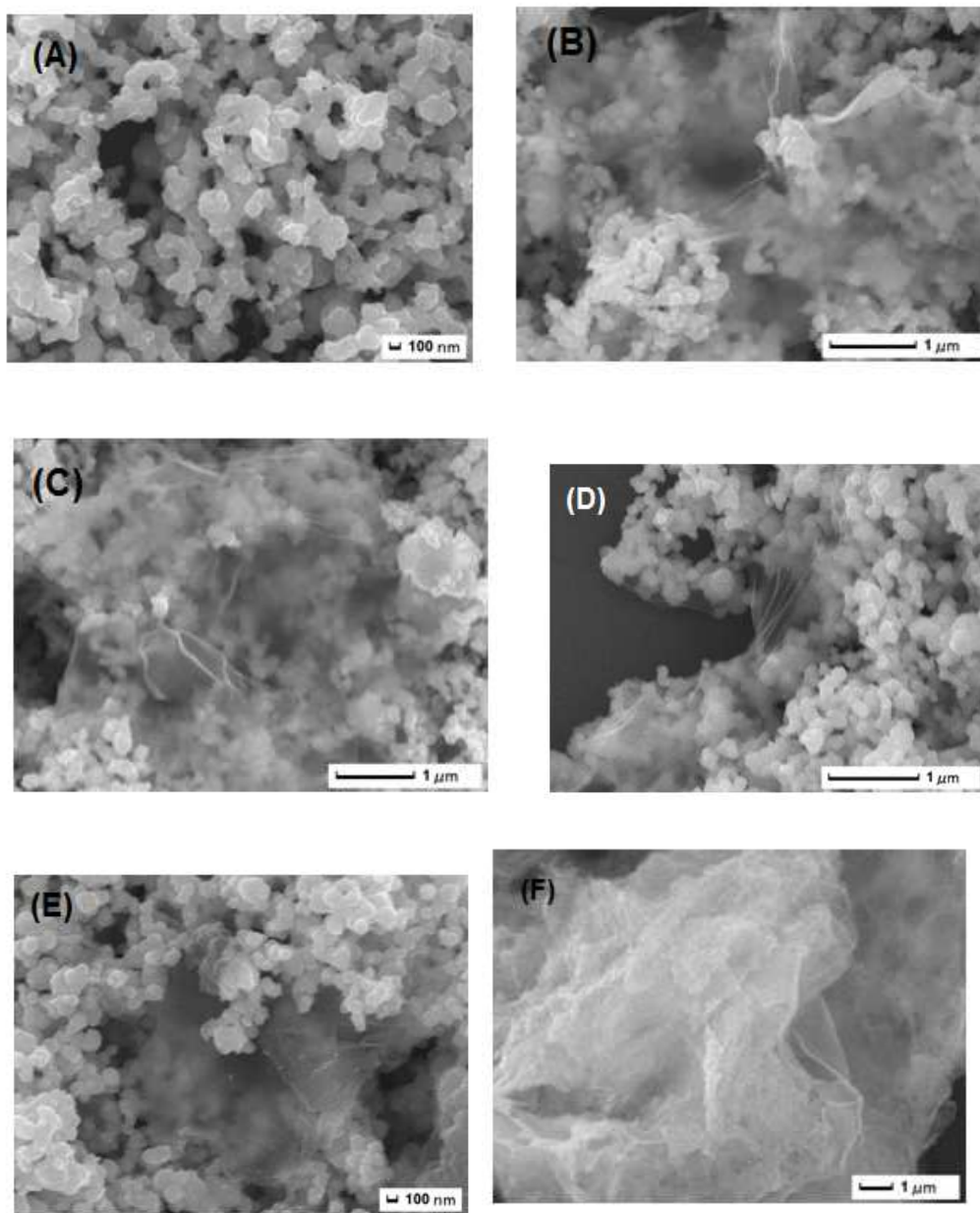


Fig. 4 SEM images of (A) pure Ag_3PO_4 , (B) graphene-analogue $\text{BN}/\text{Ag}_3\text{PO}_4$ (0.1 wt.%), (C) graphene-analogue $\text{BN}/\text{Ag}_3\text{PO}_4$ (0.5 wt.%), (D) graphene-analogue $\text{BN}/\text{Ag}_3\text{PO}_4$ (1 wt.%), (E) graphene-analogue $\text{BN}/\text{Ag}_3\text{PO}_4$ (5 wt.%), (F) graphene-analogue BN.

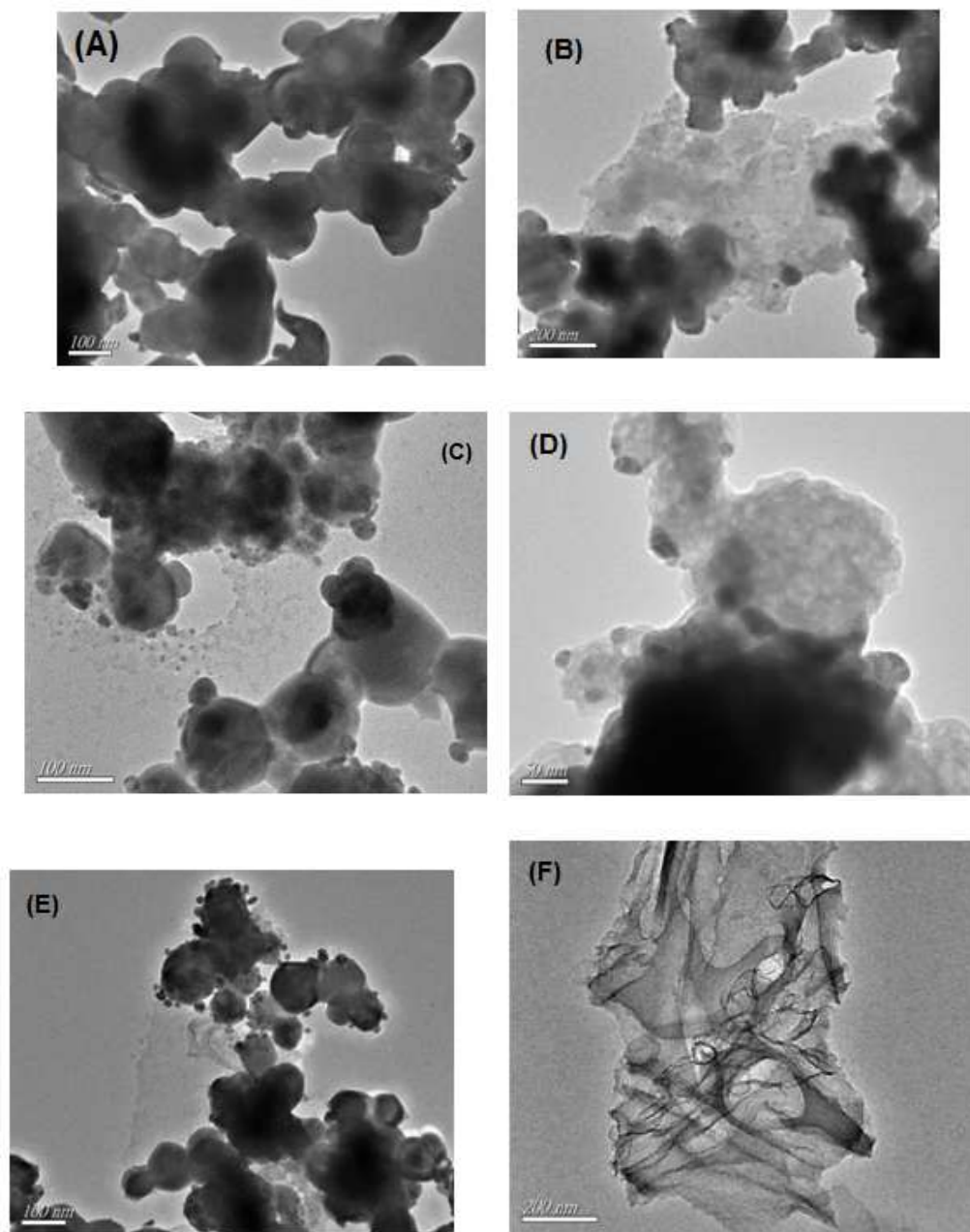


Fig. 5 TEM images of (A) pure Ag_3PO_4 , (B) graphene-analogue $\text{BN}/\text{Ag}_3\text{PO}_4$ (0.1 wt.%), (C) graphene-analogue $\text{BN}/\text{Ag}_3\text{PO}_4$ (0.5 wt.%), (D) graphene-analogue $\text{BN}/\text{Ag}_3\text{PO}_4$ (1 wt.%), (E) graphene-analogue $\text{BN}/\text{Ag}_3\text{PO}_4$ (5 wt.%), (F) graphene-analogue BN.

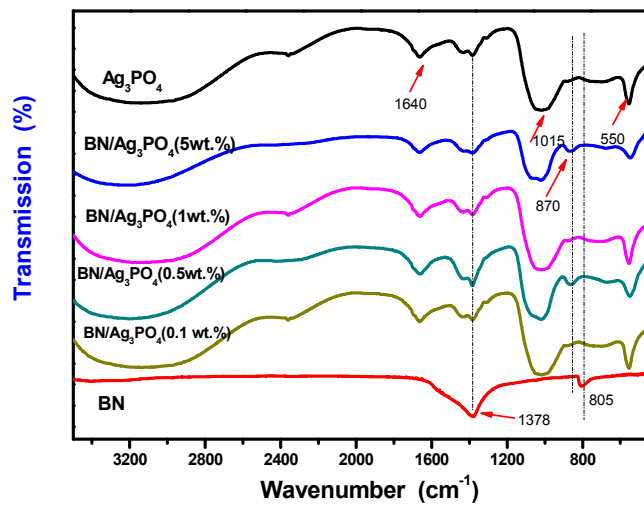


Fig. 6 FT-IR spectra of the graphene-analogue BN/Ag₃PO₄ composites.

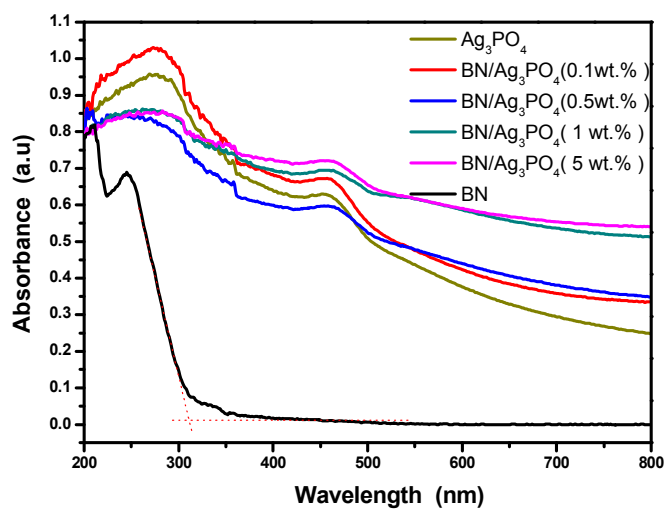
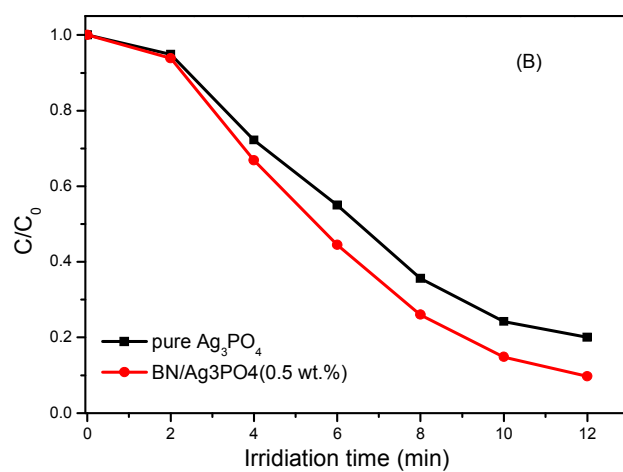
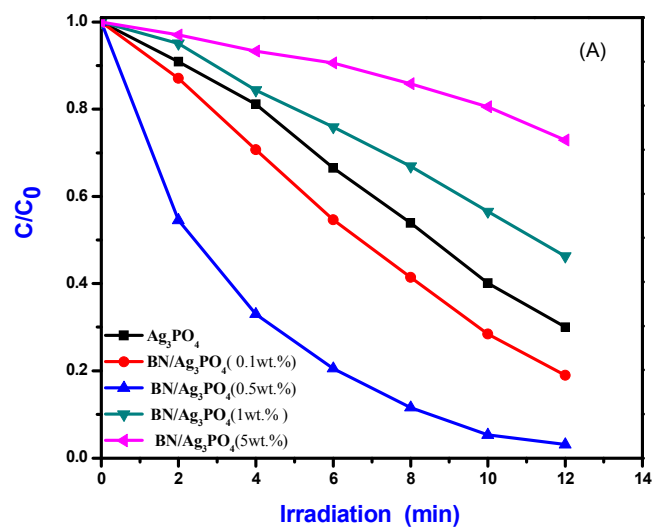
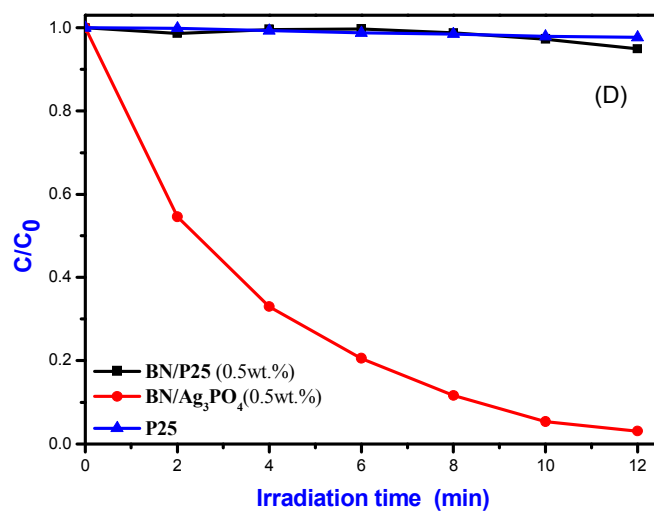
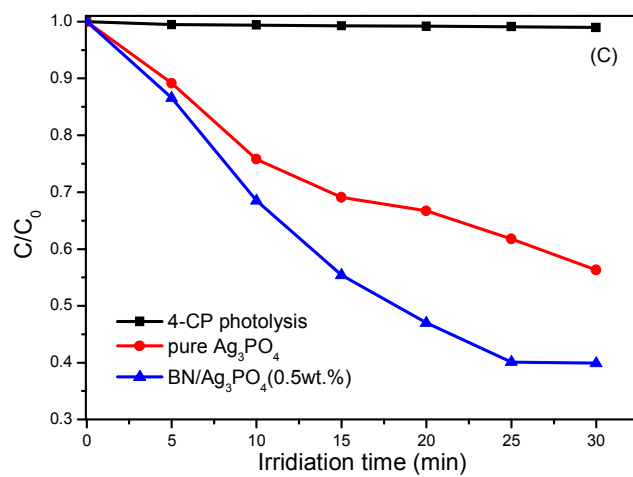


Fig.7 UV-Vis absorption spectra of BN, Ag_3PO_4 , and the graphene-analogue $\text{BN}/\text{Ag}_3\text{PO}_4$ composites with various BN contents.





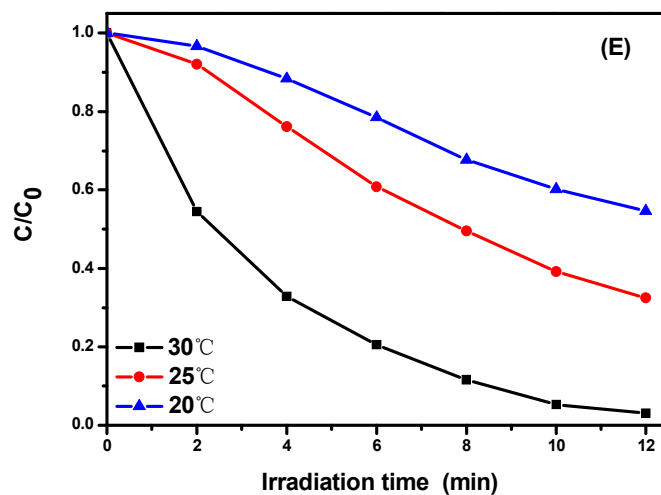


Fig.8 Photocatalytic efficiency in the case of Ag_3PO_4 and $\text{BN}/\text{Ag}_3\text{PO}_4$ for (A) RhB degradation, (B) MB degradation, (C) 4-CP degradation under visible light irradiation; (D) Compared the photocatalytic activity with other materials(for RhB degradation), (E) Photocatalytic degradation efficiency of RhB at different reaction temperature.

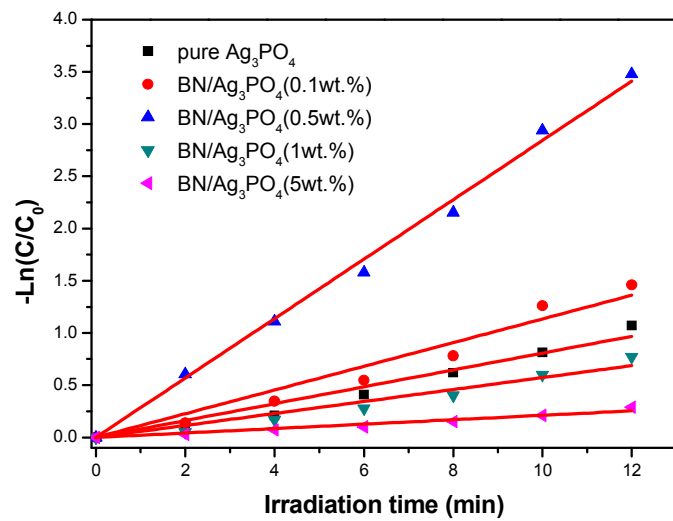


Fig.9 First-order kinetics data for the photodegradation of RhB over Ag_3PO_4 and $\text{BN}/\text{Ag}_3\text{PO}_4$ samples.

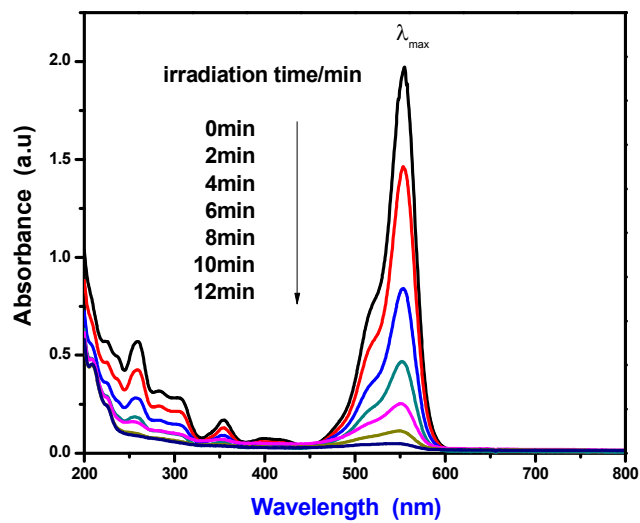


Fig. 10 Absorption spectra of RhB after different irradiation times in the presence of graphene-analogue BN/Ag₃PO₄(0.5 wt.%).

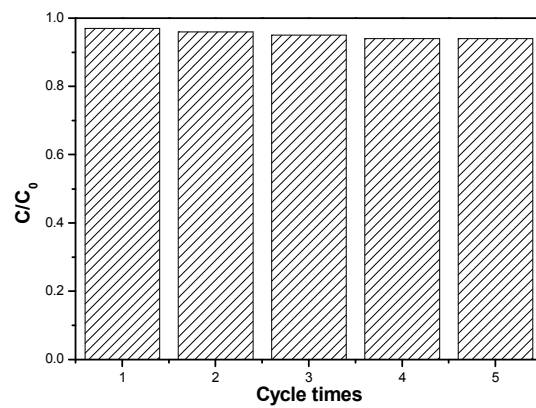


Fig. 11 Cycling runs for photocatalytic degradation of RhB over graphene-analogue BN/Ag₃PO₄ composite (0.5 wt.%).

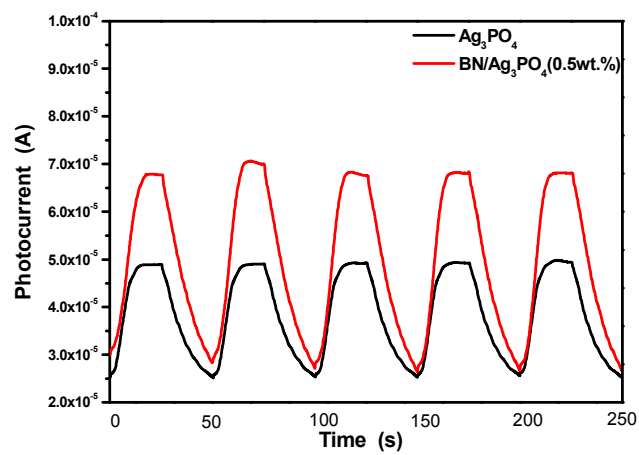


Fig. 12 Photocurrent responses of Ag_3PO_4 and graphene-analogue $\text{BN}/\text{Ag}_3\text{PO}_4$.

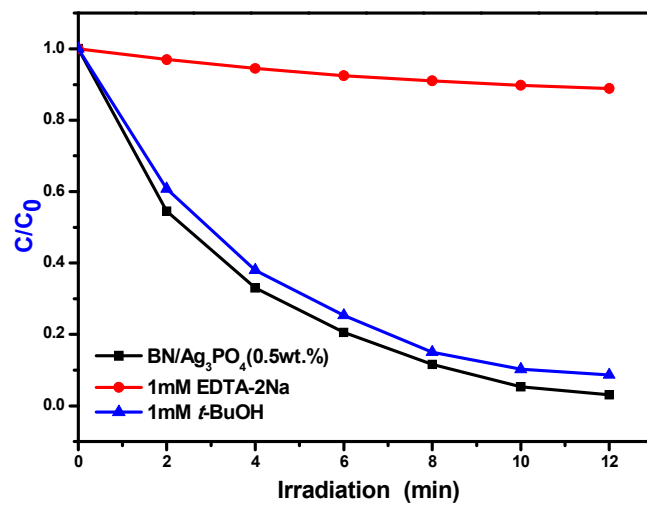


Fig. 13 Photocatalytic degradation experiments with the addition of hole and radical scavenger.

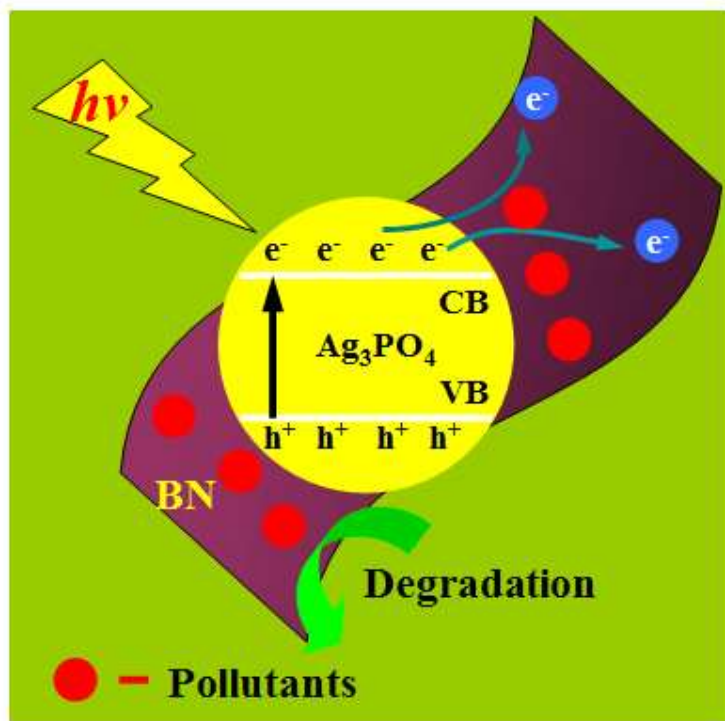


Fig. 14 The proposed photocatalytic mechanism of graphene-analogue BN/Ag₃PO₄ composite.